

Influence of alloying elements and cooling rate on the presence of delta ferrite in modified 9Cr–1Mo as-welded microstructure produced by gas–metal arc welding

S. S. Mahlalela¹, P. G. H. Pistorius²

South African Institute for Welding Centre for Welding Engineering, Department of Materials Science and Metallurgical Engineering, University of Pretoria, Gauteng, South Africa

Corresponding author: ¹Sibusiso. S. Mahlalela
Email: ¹sibusiso.mahlalela@up.ac.za ²pieter.pistorius@up.ac.za
ORCID iD: ¹0000-0002-9504-4705 ²0000-0001-6582-8157

ABSTRACT

Although P91 steel welds should ideally exhibit a fully martensitic microstructure, delta ferrite is sometimes observed, which has detrimental effects on mechanical properties and performance during application. This research focused on the role of various alloying elements on the occurrence of delta ferrite in the final weld metal. In addition, a few welds were deposited using a preheating temperature of 250 °C to investigate the effect of slower cooling rates. Of 28 gas–metal arc welds with systematic variation in chemical composition, 21 welds fully complied with the AWS A5.28/A5.28M:2020 composition specification and 18 welds contained delta ferrite in their final microstructure. Of the 18 welds with delta ferrite, 13 complied with the composition specification. The results clearly demonstrate that compliance of weld metal chemical composition to the AWS A5.28/A5.28M:2020 specification does not ensure a fully martensitic as-welded microstructure. A larger ($A_{e4} - A_{e3}$) temperature range, which is the region where only austenite phase is stable, allows more time for delta ferrite to transform to austenite during cooling. The ($A_{e4} - A_{e3}$) value necessary to suppress delta ferrite in the as-welded microstructure decreased when preheating was applied. These results indicate that both the chemical composition, which determines the ($A_{e4} - A_{e3}$) value, and the cooling rate through this temperature range are important in suppressing delta ferrite in the final as-welded microstructure.

Keywords: 9Cr–1Mo (P91) steel, delta ferrite, gas–metal arc welding, laser metal deposition, predictive empirical formulae

1. INTRODUCTION

Modified 9Cr–1Mo steel, also known as P91, was first developed at Oak Ridge National Laboratories, USA, under the designation P9. The P9 steel was modified by addition of carbo-nitride-forming elements, such as niobium and vanadium, and a limited amount of nitrogen [1]. The modified 9Cr–1Mo (P91) alloy has a martensitic microstructure, which provides excellent properties for long-term high-temperature applications as boiler and turbine materials in power-generating plants [2].

Delta ferrite is the primary phase that transforms from liquid at the start of solidification in P91 steel, as shown in the P91 compositional equilibrium phase diagram constructed using Thermo-Calc software (Fig. 1) [3], where the broken red line indicates the average chromium content. Delta ferrite transforms to austenite which subsequently transform to martensite with further cooling during fabrication. The ($A_{e4} - A_{e3}$) temperature range highlighted in Fig. 1 is the region where only austenite phase is stable under equilibrium conditions. A_{e4} temperature indicates the completion of delta ferrite to austenite transformation and A_{e3} the onset of alpha ferrite transformation under equilibrium conditions on cooling. P91 final weld microstructure sometimes exhibits delta ferrite, which is detrimental to mechanical properties and performance during application [4]. The reason for this occurrence is that delta ferrite formed at temperatures above A_{e4} often does not transform completely to austenite during subsequent cooling during welding. The presence of delta ferrite in the final microstructure is influenced by the ($A_{e4} - A_{e3}$) temperature range which is determined by the balance between ferrite- and austenite-forming elements. Arivazhagan and Kamaraj [5] stated that the chance of delta ferrite retention in a weld increases with a

lower value of $(Ae_4 - Ae_3)$. A larger $(Ae_4 - Ae_3)$ value means that austenite is stable over a wider range of temperature and that delta ferrite has more time to transform to austenite during cooling [3].

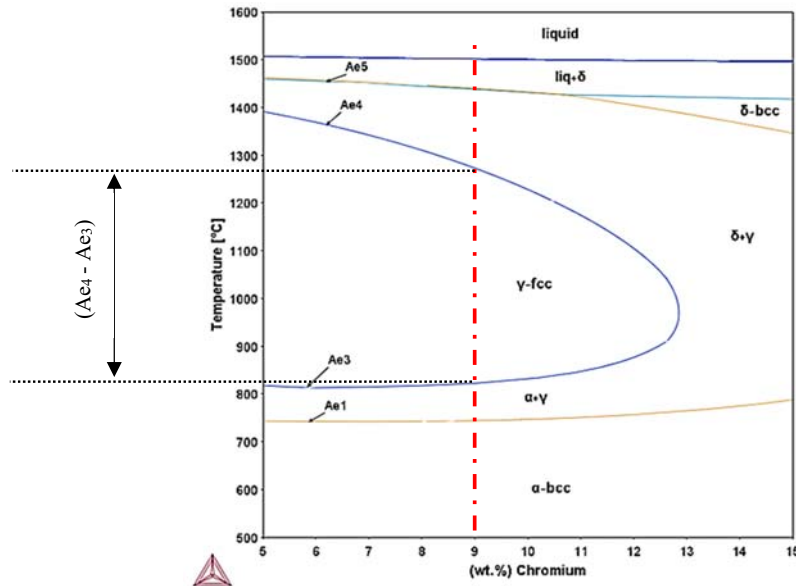


Fig. 1 P91 compositional phase diagram in the 5 to 15 mass% chromium range, showing the $(Ae_4 - Ae_3)$ region [3].

1.1 Role of alloying elements in P91 steel

During this study, five alloying elements (Cr, Ni, Mn, Si, and Mo) were varied in the weld metal. The role of these elements in P91 steel are considered below.

Chromium (Cr) is an essential element in P91 steel because of its effect in improving creep strength and corrosion and oxidation resistance for elevated-temperature application by solid-solution strengthening and precipitation [6]. Chromium is also a ferrite-stabilising element and thus has a strong influence on the ferrite factor (FF) and in suppressing the delta ferrite-austenite transformation temperature (Ae_4). Increasing the chromium content therefore reduces the “austenite-only” region ($Ae_4 - Ae_3$), which increases the potential for delta ferrite presence in the final microstructure [7].

Nickel (Ni) is a strong austenite former. An increase of nickel in P91 steel widens the $(Ae_4 - Ae_3)$ temperature range and lowers the Ae_1 temperature. These factors ensure complete austenitic transformation, which translates to a fully martensitic final microstructure [8]. Ae_1 temperature indicates the onset of austenite formation on heating. Nickel addition brings the Ae_1 temperature closer to the post-weld heat-treatment (PWHT) temperature, therefore care must be taken to ensure that Ae_1 is not so low that PWHT causes some austenite to form, which upon cooling will transform to fresh martensite [9]. Excess amounts of nickel can also adversely affect the creep properties of P91 steel because it promotes the formation of $M_6(C,N)$, which exhibits a high coarsening rate at elevated temperatures thus destabilising the $M_{23}C_6$ precipitates during service [10]. As a consequence, a 1% Ni maximum limit is recommended [9].

Manganese (Mn) is an austenite stabiliser and, together with nickel, lowers the Ae_1 temperature and martensite start and finish temperatures [11]. Manganese and nickel are very effective in preventing the retention of delta ferrite, but their total amount ($Mn + Ni$) in the weld metal is limited to 1.5% maximum as a safeguard against austenite reformation during PWHT [9].

Silicon (Si) is a ferrite stabilizer. Increasing its content in the P91 weld metal will result in a higher volume fraction of delta ferrite in the microstructure [8]. Increasing the amount of silicon was also reported to influence the morphology of delta ferrite phase [4]. Silicon is a deoxidant and, together with chromium, may contribute to oxidation resistance [9].

Molybdenum (Mo) is a ferrite stabiliser and thus must be limited to avoid delta ferrite presence in the final weld microstructure. Molybdenum increases the upper and lower critical temperatures (A_{e3} and A_{e1} , respectively), which reduces the austenite-only region [12]. Molybdenum contributes significant solid–solution strengthening, but excessive molybdenum can be detrimental in long-term creep strength through the formation of Fe_2Mo Laves phase that depletes the molybdenum in solution [10].

1.2 Empirical formulae to predict the final microstructure

Empirical formulae that reflect the balance between austenite- and ferrite-forming elements are used in the design of P91 weld composition to avoid the presence of delta ferrite in the as-welded microstructure. The two most commonly used predictive empirical formulae for P91 steel welds are the modified Schneider formulae (Equations 1 and 2) [13]:

$$Cr_{eq} = Cr + 2Si + 1.5Mo + 5V + 1.75Nb + 0.75W; \quad (1)$$

$$Ni_{eq} = Ni + 0.5Mn + 30C + 25N + 0.3Cu, \quad (2)$$

and the Kaltenhauser formula (Equation 3) [14]:

$$\text{Kaltenhauser ferrite factor (KFF)} = Cr + 6Si + 4Mo + 4Nb + 2Al + 8Ti - 2Mn - 2Ni - 40(C + N). \quad (3)$$

A convenient approach to presenting the Schneider formulae is through the use of the ferrite factor (FF), which is the difference between the chromium and nickel equivalents ($Cr_{eq} - Ni_{eq}$) [15]. The main difference between these formulae is the increased weighted effects of Si and Mo and additions of Ti and Al to the Kaltenhauser formula. To obtain a weld metal free from delta ferrite, Onoro [16] stated that a Schneider chromium equivalent (Cr_{eq}) value lower than 13.5 and FF lower than 8 are necessary. Sireesha [14] recommended that the Kaltenhauser FF should have a maximum value of 8 to avoid ferrite retention in P91 welds.

Using the chromium–nickel balance (CNB) formulation (Equation 4) from a modified Newhouse’s equation, Swindeman et al. [17] stated that delta ferrite is not usually present if the CNB is less than 10; for CNB above 12, significant quantities of delta ferrite are observed [17]:

$$CNB = Cr + 6Si + 4Mo + 1.5W + 5Nb + 9Ti + 11V + 12Al - 40C - 30N - 2Mn - 4Ni - Cu. \quad (4)$$

Weld microstructure prediction methods and related research have been extensively studied to improve their accuracy in different alloys [18]. Significant progress has been reported, but delta ferrite in P91 as-welded microstructures is observed in alloys with Cr_{eq} and FF values well below the recommended values [19, 20].

1.3 Effect of cooling rate on delta ferrite during welding

The cooling rate during welding is mainly influenced by the heat input and the pre-heat temperature. Sam et al. [21] studied the effect of cooling rate in weld metal with a composition containing 9% Cr by varying the heat input between 1 to 2 kJ/mm and applied different pre-heats varying from no pre-heat, to 100 °C and 200 °C at constant heat input. The results showed that a slower cooling rate, achieved by higher pre-heat temperature and heat input, reduced the delta ferrite observed in the final microstructure [21]. Onoro [16] and Faulkner et al. [13] also observed smaller amounts of delta ferrite in P91 shielded-metal arc welds (SMAW) at slower cooling rates.

A similar effect of cooling rate on retained delta ferrite was reported by Zhou et al. [22] from dilatometric experiments using P92 alloy. The samples were rapidly heated to a peak temperature of 1350 °C and then cooled at various cooling rates. Between 30 and 50 °C/s, a small increase in retained delta ferrite was observed; at a cooling rate of 200 °C/s, the delta ferrite volume fraction was significantly higher, as shown in Fig. 2[22]. At a very slow cooling rate of 1 °C/s, the austenite-to-delta ferrite transformation persisted above the Ac_4 temperature because of the large proportion of austenite relative to the equilibrium fraction. Consequently, the starting amount of delta ferrite increased, which accounts for the high volume fraction of delta ferrite reported in Fig. 2 for 1 °C/s cooling rate. The observations of Zhou et al. [22] are applicable to the heat affected zone in multi-pass welding where prior beads are reheated above the Ac_4 temperature.

At very fast cooling rates during solidification, delta ferrite nucleation can be suppressed, leading to a decrease in the amount of delta ferrite formed from liquid and, therefore, more austenite forms directly from the supercooled liquid [21, 23]. The change in solidification mode of the primary phase from ferrite only to ferrite + austenite explains the observation of Arivazhagan et al. [7], shown in Fig. 2, that delta ferrite in the final weld microstructure decreased with increasing cooling rate.

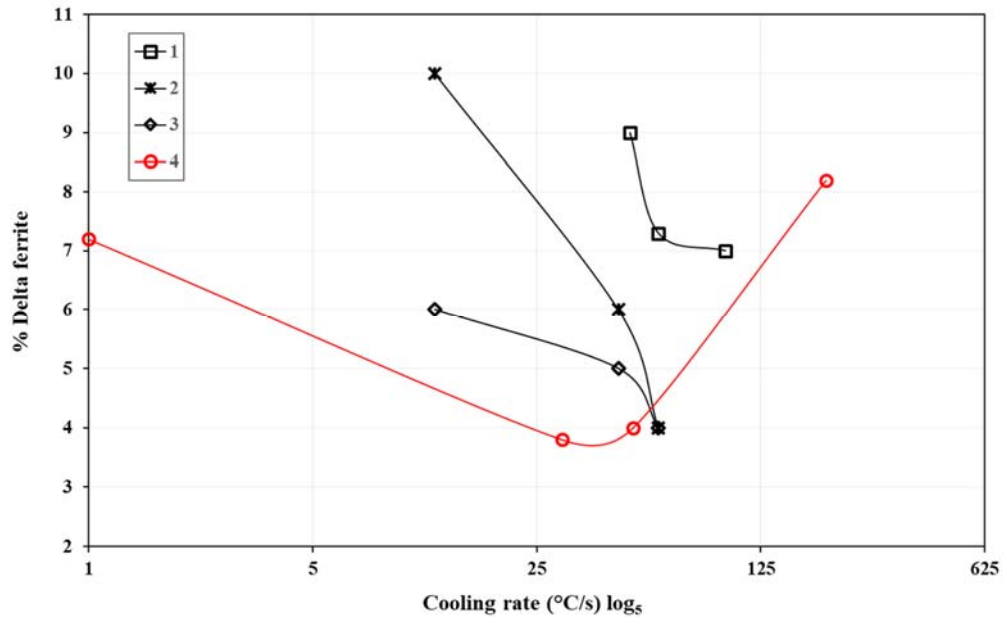


Fig. 2 Published data on the effect of cooling rate on delta ferrite volume fraction. Graphs 1,2 and 3 are results published by Arivazhagan from GTA welds [7] (key to data: 1: Butt joint with filler wire; 2: Autogenous bead on plate; 3: Autogenous butt joint). Graph 4 are results reported by Zhou et al. [22] from dilatometric experiments.

support the generally accepted observation that P91 welds show an increase in delta ferrite volume fraction with faster cooling rates. This is due to the fact that the time available for the austenite to delta ferrite transformation through the ($A_{e4} - A_{e3}$) temperature range is reduce with increasing cooling rate. Contradictory results can nevertheless be observed, as can be seen in Fig. 2 with Arivazhagan results that show decreased delta ferrite in the final weld microstructure with increasing cooling rate due to the change in solidification mode.

2. EXPERIMENTAL PROCEDURE

2.1 Base material and filler wire

This research focused on the role of various alloying elements on the amount of delta ferrite in the final weld metal of modified 9Cr–1Mo alloy. The objective was to determine if delta ferrite can be observed in as-welded microstructures of P91 weld metal that fully complies with the chemical composition requirements of the American Welding Society (AWS) A5.28/A5.28M:2020 and International Standards Organisation (ISO) 21952:2007 (CrMo91) standards. Selected welds were deposited using an elevated-temperature preheating (250 °C) treatment to investigate the effect of slower cooling rate on the delta ferrite content in the as-welded condition.

A seamless pipe of X10CrMoVNb9-1(P91) steel grade was used as the base material. A small thickness of material was skimmed from the outside of the pipe to remove any rust or contamination and to ensure a smooth surface on which the weld beads were deposited. The final dimensions of the pipe were 245 mm outside diameter, a thickness of 29 mm, and a length of 330 mm. Table 1 shows the chemical composition of the base material. A 1 mm diameter Böhler C 9 MV-UP was used as the gas–metal arc welding (GMAW) filler material; its chemical composition, as provided by the supplier, is shown in Table 2. The supplier’s inspection certificate stipulated that the chemical composition was for hot-rolled wire with heat number 101798. The AWS A5.28/A5.28M and ISO 21952:2020 (CrMo91) specifications are included in Table 2 for the purposes of comparing the two standards.

Table 1. Chemical composition (%) of P91 base material steel pipe (ASTM A335/A335M-21)

ASTM A335/A335M-21	C	Mn	Cr	Si	Mo	V	Nb	N	Ni	Al
		0.08–0.12	0.30–0.60	8.0–9.5	0.20–0.50	0.85–1.05	0.18–0.25	0.06–0.10	0.03–0.07	0.4 max
Base material	0.11	0.53	8.21	0.33	0.93	0.24	0.10	0.06	0.25	0.005

Table 2. Böhler C 9 MV-UP filler wire chemical composition (%), as provided by the supplier (AWS A5.28/A5.28M:2020 and ISO 21952:2007 (CrMo91) specification)

AWS A5.28/A5.28M	C	Mn	Cr	Si	Mo	V	Nb	N	Ni	Al	Cu
		0.07–0.13	1.20 max	8.0–10.5	0.15–0.50	0.85–1.20	0.15–0.30	0.02–0.10	0.03–0.07	0.8 max	0.04 max
ISO 21952 (CrMo91)	0.07–0.15	0.4–1.5	8.0–10.5	0.6 max	0.80–1.20	0.15–0.30	0.03–0.10	0.02–0.07	0.4–1.0	-	0.25 max
Filler wire	0.10	0.60	8.80	0.24	0.94	0.20	0.06	0.04	0.50	-	0.03

Systematic variations in chemical composition of the GMAW beads were achieved by preliminary deposition of single or multiple laser beam welds of different alloying metal powders prior to overlaying them with a single-pass GMA weld (Fig. 3(i)). The laser beads were deposited according to a specific target composition, with the aim of achieving a GMAW bead that met the requirements of the AWS A5.28/A5.28M specification. A total of twenty-eight GMA welds with varying compositions were deposited along the length of the P91 steel pipe, as shown in Fig. 3(ii). The section indicated by the red arrow in Fig. 3(ii) was used for the chemical analysis and metallography results presented in this paper.

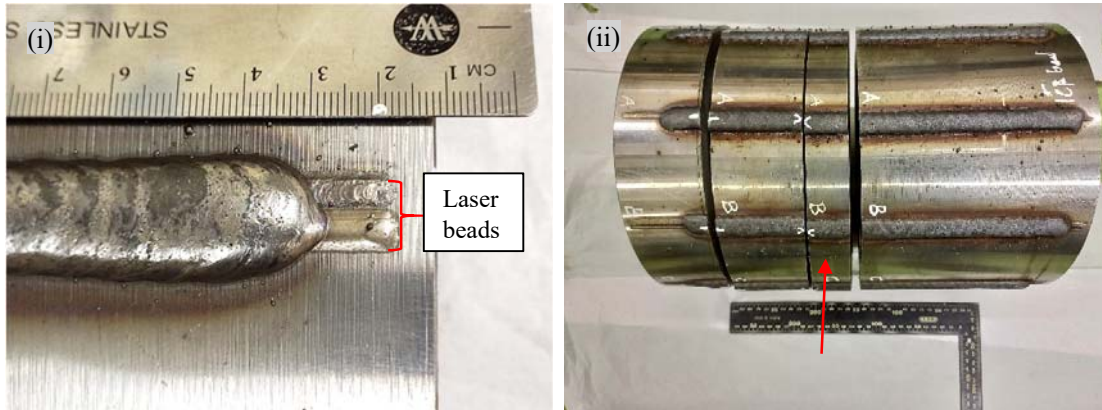


Fig. 3 Image (i) shows the laser beads overlaid by a GMAW bead. Image (ii) shows the P91 pipe with GMAW beads. The section indicated by the red arrow was removed for chemical analysis and metallography.

2.2 Laser metal deposition

Metal alloy powder was deposited on the P91 base material using an IPG YLR 3000-ST fibre laser with a maximum power output of 3 kW. The welding head that houses the nozzle through which the metal powder was fed directly into the weld pool was mounted on an articulated arm robot. Argon was used as the shielding gas at a flow rate of 1.2 l/min. Table 3 shows the metal alloy powders added and laser beam welding parameters.

Table 3. Metal powders used for alloying and laser beam welding parameters

Metal alloy powder		Laser beam welding parameters			
Name	Composition	Spot size (mm)	Laser power (kW)	Laser speed (m/min)	Powder feed speed
TLS (Cr99.2)	99.2% Cr	4	2.0	0.5	1.4 rpm: 4.00 g/min
METCO 56C-NS (Ni powder)	99.3% Ni	2	1.2	1.2	1.5 rpm: 4.05 g/min
Weartech (Mo99.5)	99.5% Mo	2	1.2	1.2	1.2 rpm: 3.90 g/min
Manganese Metal Co powder	99.8 % Mn	2	1.0	1.2	2.5 rpm: 2.13 g/min
FeSi (6F)	16.6% Si and 82.5% Fe	4	2.2	0.5	1.4 rpm: 2.10 g/min

2.3 Gas–metal arc welding

All gas–metal arc welds were bead-on-plate welds undertaken using the parameters shown in Table 4. Six welds were performed at a preheat temperature of 250 °C, designated PH1 to PH6. Twenty-two additional welds, designated AW1 to AW22, did not receive any preheating. The average cooling rate at the fusion line of the welds was calculated from the cooling time (Δt_{12-8}) based on Rosenthal equation. The estimated cooling rates of the preheated welds and the non-preheated welds were 60 and 95 °C/s respectively. The welding process was semi-automated, with the torch clamped to an arm that was controlled by the rail-runner welding carriage. The carriage comprised an oscillator that permitted a weaving welding path to be applied to ensure wider GMAW beads to sufficiently cover the laser alloying beads. The shielding gas was argon with 2% oxygen at a flow rate of 15 l/min.

Table 4. Welding parameters used for GMAW beads

Process Variables	Parameters (No pre-heat)	Parameters (Pre-heat @ 250 °C)
Welding speed (cm/min)	20	20
Wire feed speed (m/min)	13.2	13.2
Welding current (A)	218 average	218 average
Welding voltage (V)	28.5 average	31.5 average
Contact tip to work distance (mm)	20	20
Welding Path	Weaving (Trapezoid)	Weaving (Trapezoid)
Oscillation width (mm)	7	7
Oscillation position delay (s)	0.3	0.3
Oscillation travel speed (cm/min)	20	20
Heat Input (kJ/mm) (0.85 arc efficiency)	1.4 - 1.7	1.7
Average weld cooling rate (°C/s) (estimated from Δt_{12-8})	95	60

2.4 Characterization

The weld beads were sectioned in the transverse and longitudinal planes for metallographic analysis using a stereoscope (Olympus SZX7) and optical microscope (Olympus BX51M). Etching was achieved using Vilella’s reagent (100 ml ethanol, 1 g picric acid, 5 ml hydrochloric acid) [20]. Delta ferrite phase fraction was quantified by analysing micrograph images of the welds using ImageJ software. Over 20 micrograph images per weld were analysed, taken at 100× magnification and covering the transverse cross-section of the weld. A 95% confidence interval for the estimated delta ferrite content was calculated from the average and the standard deviation of these measurements [25].

3. RESULTS AND DISCUSSION

3.1 Chemical compositions of welds

Chemical compositions of the GMAW beads were analysed using optical emission spectrography. The chemical composition and delta ferrite measurements were performed on the two opposite planes obtained from the transverse sectioning of the welds. Table 5 presents the alloying elements added on each GMAW bead and the final chemical composition. Welds PH1 and AW1 comprised only the GMAW deposit (i.e., without any laser metal beads). Seven welds, highlighted in Table 5, did not fully comply with the AWS A5.28/A5.28M:2020 specification. This standard does not specify minimum requirements for Mn or Ni, but does specify that the sum (Mn + Ni) shall be less than or equal to 1.5% maximum. Welds AW7, AW8, and AW11 were above the required limit of 1.5% (Mn + Ni). Manganese and nickel are both austenite stabilisers/formers and their presence in the weld metal is crucial in limiting delta ferrite presence in the final weld microstructure. An equivalent standard to the AWS A5.28 is ISO 21952, which specifies minima of 0.4% Mn and 0.4% Ni.

Table 5. Metal alloys deposited and actual composition (%) of GMAW beads (AWS A5.28/A5.28M:2020 specification). Elements above the specified limit are highlighted.

GMAW beads	Alloying added (laser beads deposited)	C	Mn	Cr	Si	Mo	V	Nb	N	Ni	Al	(Mn+Ni)
		0.08-0.13	1.20 max	8.0-10.5	0.5 max	0.85-1.2	0.15-0.30	0.02-0.10	0.03-0.07	0.8 max	0.04 max	1.5 max
250 °C Pre-heat												
PH 1	No Alloying	0.090	0.48	8.40	0.28	0.97	0.22	0.081	0.052	0.35	0.005	0.83
PH 2	(0.5)Cr	0.089	0.47	8.88	0.28	0.97	0.22	0.077	0.051	0.36	0.004	0.83
PH 3	(1)Cr	0.087	0.47	9.47	0.28	0.97	0.22	0.078	0.054	0.36	0.005	0.83
PH 4	(2)Cr, (2)Mn	0.085	1.08	10.01	0.28	0.96	0.22	0.079	0.053	0.34	0.005	1.42
PH 5	(2)Cr, (1)Mn, (1)Mo	0.085	0.75	10.33	0.28	1.32	0.22	0.078	0.055	0.34	0.006	1.09
PH 6	(1)Cr, (1)Mn, (0.5)Ni	0.087	0.81	9.39	0.27	0.96	0.22	0.079	0.053	0.52	0.003	1.33
No Pre-heat												
AW 1	No Alloying	0.090	0.48	8.61	0.31	0.94	0.22	0.088	0.056	0.35	0.003	0.83
AW 2	(1)Cr	0.100	0.48	9.12	0.30	0.93	0.21	0.082	0.055	0.35	0.004	0.83
AW 3	(2)Cr	0.100	0.49	10.31	0.29	0.94	0.22	0.086	0.059	0.36	0.010	0.85
AW 4	(2)Cr, (0.5)Mo	0.094	0.47	10.22	0.25	1.05	0.22	0.082	0.065	0.36	0.003	0.83
AW 5	(2)Cr, (1)Mo	0.090	0.48	10.18	0.30	1.37	0.22	0.088	0.057	0.35	0.006	0.83
AW 6	(2)Cr, (0.5)Ni	0.089	0.47	10.25	0.24	0.94	0.23	0.082	0.070	0.54	0.003	1.01
AW 7	(2)Cr, (1)Ni	0.100	0.48	10.30	0.30	0.91	0.22	0.083	0.057	1.13	0.005	1.61
AW 8	(2)Cr, (2)Ni	0.080	0.48	10.19	0.28	0.90	0.21	0.085	0.057	1.39	0.006	1.87
AW 9	(2)Cr, (1)Si	0.088	0.46	9.95	0.47	0.92	0.23	0.086	0.069	0.34	0.005	0.80
AW 10	(2)Cr, (2)Si	0.080	0.47	10.09	0.69	0.89	0.22	0.089	0.056	0.34	0.006	0.81
AW 11	(2)Cr, (2)Mn	0.100	1.16	9.74	0.29	0.92	0.22	0.083	0.059	0.35	0.004	1.51
AW 12	(2)Mn, (0.5)Mo	0.091	1.11	8.39	0.24	1.13	0.23	0.080	0.062	0.36	0.002	1.47
AW 13	(1)Mn, (1)Si	0.088	1.12	8.38	0.42	0.95	0.23	0.084	0.063	0.36	0.002	1.48
AW 14	(0.5)Mo, (1)Si	0.085	0.47	8.42	0.48	1.05	0.23	0.083	0.061	0.35	0.003	0.82
AW 15	(2)Cr, (0.5)Mo, (1)Si	0.085	0.46	9.18	0.45	1.02	0.23	0.089	0.060	0.35	0.004	0.81
AW 16	(2)Cr, (1)Mo, (1)Si	0.082	0.46	9.81	0.45	1.15	0.23	0.086	0.060	0.35	0.003	0.81
AW 17	(2)Cr, (1)Mo, (2)Si	0.100	0.46	9.92	0.58	1.20	0.22	0.085	0.056	0.34	0.005	0.80
AW 18	(2)Cr, (0.5)Mo, (1)Mn	0.102	0.79	10.26	0.23	1.02	0.22	0.078	0.070	0.36	0.003	1.15
AW 19	(2)Cr, (1)Mo, (1)Mn	0.120	0.91	9.71	0.29	1.34	0.22	0.086	0.059	0.34	0.008	1.25
AW 20	(2)Cr, (0.5)Mo, (0.5)Ni	0.088	0.47	9.55	0.25	1.03	0.23	0.083	0.059	0.54	0.003	1.01
AW 21	(2)Cr, (1)Mn, (1)Si	0.081	0.78	9.94	0.43	0.93	0.23	0.085	0.061	0.35	0.004	1.13
AW 22	(0.5)Mo, (2)Mn, (1)Si	0.081	1.13	8.27	0.50	1.04	0.23	0.088	0.065	0.35	0.003	1.48

3.2 Macrostructure

Weld beads cross-sections in the transverse and longitudinal planes are shown in Fig. 4. The uneven base-metal penetration and wave-like fusion line observed along the length of the weld bead in Fig. 4(ii) are attributed to the weaving technique. The depth of penetration varied from 2.5 to 3.6 mm and the bead width varied from 14.1 to 17.5 mm between the welds. The weld dilution, which is the ratio of the molten base metal to the total fusion zone, varied from 26% to 40%. Use of the weaving technique in GMAW is effective in increasing the weld width and heat input. No significant effect of preheating was observed on the geometry of the weld bead. Differences in weld bead geometry and dilution between the weld beads were attributed, but not limited, to the elements and number of laser beads added. The weaving technique in GMAW is effective in increasing the weld width and heat input, but results in an uneven fusion line, which makes accurate weld geometry calculation difficult.

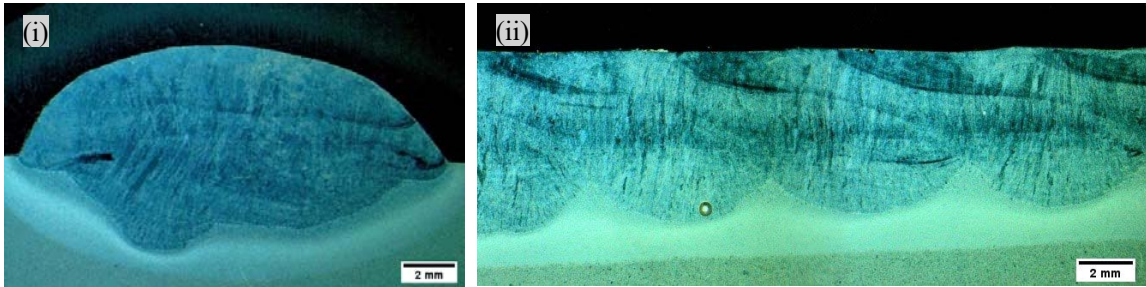


Fig. 4 Stereoscope images of weld bead cross-section in the transverse (image (i)) and longitudinal (image (ii)) planes. Magnification 10 \times .

3.3 Optical microstructure analysis

3.3.1 250 °C preheat

Four of the six welds that received pre-heat treatment were fully martensitic, represented by weld PH2 microstructure image shown in Fig. 5(i). Welds PH4 and PH5 consisted of a martensitic matrix with 0.3% and 3.5% delta ferrite, respectively, in their final microstructure (Fig. 5(ii)). Weld PH5 contained additional molybdenum and chromium, which are both strong ferrite formers, and a single laser bead of manganese, which is an austenite stabiliser. The additional manganese in weld PH4 was insufficient to ensure complete transformation of delta ferrite to austenite during cooling. The chemical composition of all pre-heated welds, with the exception of weld PH5, conformed to the AWS A5.28/A5.28M:2020 specification.

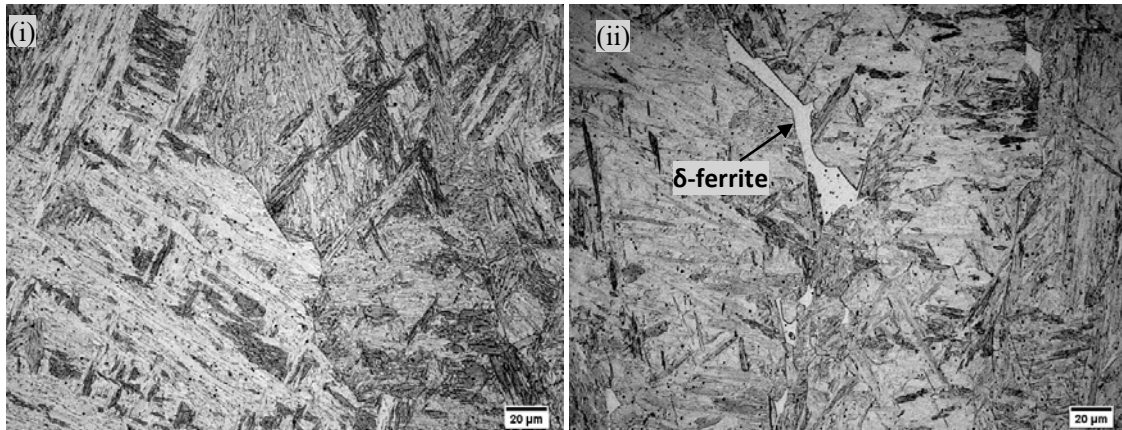


Fig 5. Optical microstructure images of preheated welds in as-welded condition taken at higher magnification (500 \times). Weld PH2, comprising a fully martensitic matrix, is shown in image (i). Weld PH5, comprising a 3.5% delta ferrite in a martensitic matrix, is shown in image (ii).

3.3.2 No pre-heat

Only six of the 22 welds (AW1, 7, 8, 12, 13, and 22) comprised a fully martensitic microstructure, represented by the image shown in Fig. 6(i). Nickel contents in welds AW7 and AW8 were above the AWS specification

limit because of the added nickel laser beads. The absence of delta ferrite in these microstructures demonstrated the strong influence of nickel on austenite formation. Welds AW12, 13, and 22 contained additional manganese, which is an austenite stabiliser, but had no additional chromium laser beads, so it was expected that delta ferrite would not be observed in the final microstructure.

Welds AW2, 11, 14, and 20 contained less than 0.5% volume fraction of small polygonal delta ferrite grains, represented by the microstructure image in Fig. 6(ii). The chemical compositions of these four welds complied with the AWS A5.28/A5.28M specification, yet their microstructure contained delta ferrite.

Figure 6(iii) shows a microstructure of weld AW19, which contained 2.4% delta ferrite in a martensitic matrix. Eight welds contained a delta ferrite volume fraction between 1% and 2.6%, and each of these welds contained laser beads of both ferrite- and austenite-forming elements. The opposing effects of these elements on delta ferrite formation was insufficient to prevent its retention in the as-welded microstructure. Six of the eight welds complied with the AWS A5.28/A5.28M composition specification.

Figure 6(iv) shows the microstructure of weld AW17, which contained 6.2% delta ferrite. The delta ferrite morphology was a mixture of small to large polygonal grains and fine elongated grains. The four remaining welds (AW5, 9, 16, and 17) contained between 3.8% to 6.2% delta ferrite. Laser beads deposited on these four welds were of chromium, molybdenum, or silicon, which are all ferrite formers. Welds AW9 and AW16 complied with the composition specification, yet contained a significant amount of retained delta ferrite.

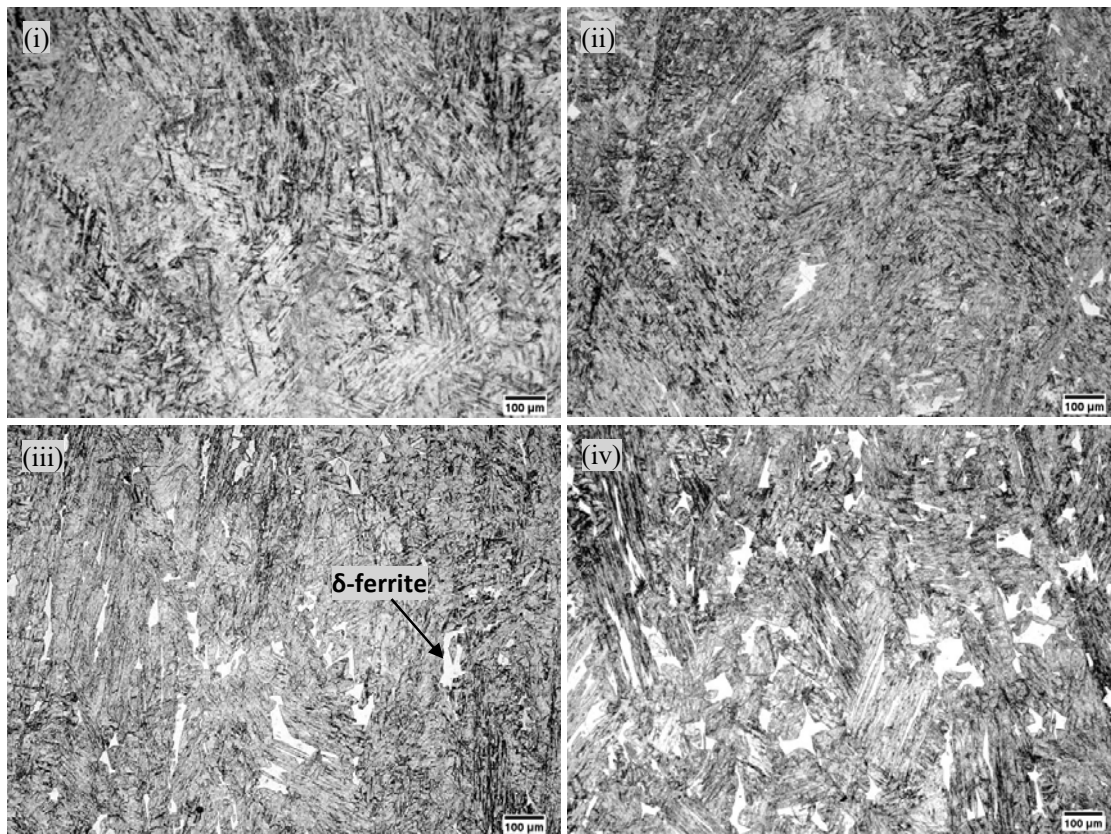


Fig. 6. Optical images of weld beads microstructures in as-welded condition. Magnification 100 \times . Image (i) is a fully martensitic weld AW8 microstructure. Image (ii) shows a microstructure of weld AW2 consisting of 0.5% delta ferrite in a martensitic matrix. Image (iii) shows a microstructure of weld AW10 consisting of 2.2 % delta ferrite. Image (iv) is a microstructure of weld AW17, which contained 6.2 % delta ferrite.

Of the 28 GMA welds investigated in this study, 21 fully complied with the AWS A5.28/A5.28M composition specification and 18 contained delta ferrite in their final microstructure. Of the 18 welds with delta ferrite, 13 met the AWS composition specification. These results clearly demonstrate that compliance of weld metal chemical composition to the AWS A5.28/A5.28M:2020 and EN ISO 21952-A CrMo91 specification ranges does not ensure a fully martensitic as-welded microstructure.

3.4 Use of empirical formulae to predict the presence of delta ferrite

The potential for delta ferrite presence in the as-welded final microstructure of modified 9Cr–1Mo steel can be estimated using empirical formulae. Table 6 presents the values calculated using the empirical formulae from Schneider [13], Kaltenhauser [14], and Newhouse [17] based on the actual weld chemical compositions. The percentage volume fraction of delta ferrite with a 95 percent confidence interval observed in each weld is also presented in Table 6.

When considering the Schneider, Kaltenhauser, and CNB evaluations together, the presence or absence of delta ferrite in the final weld microstructure was accurately predicted for 23 of the 28 welds. The microstructures of welds AW2, 11, 18, and 20 contained small amounts of delta ferrite, although all empirical formulae predicted a microstructure free from delta ferrite.

Table 6. Ferrite factor ($Cr_{eq} - Ni_{eq}$), chromium–nickel balance (CNB), and observed percentage of delta ferrite in weld microstructure (95% confidence interval). Values above the recommended limits (indicative of the risk of delta ferrite) are highlighted in red

Weld ID	Schneider			Kaltenhauser	Newhouse	% Delta - ferrite	Weld microstructure prediction
	Cr_{eq} (≤ 13.5)	Ni_{eq}	FF (≤ 8)	KFF (≤ 8)	CNB (≤ 10)	$\pm 95\% \text{ CI}$	
250 °C Pre-heat							
PH 1	11.7	4.6	7.0	7.0	9.3	0.0	✓
PH 2	12.1	4.6	7.6	7.5	9.8	0.0	✓
PH 3	12.7	4.6	8.1	8.1	10.4	0.0	✗
PH 4	13.2	4.8	8.5	7.5	9.8	0.3 ± 0.1	✓
PH 5	14.1	4.7	9.4	9.8	12.2	3.5 ± 0.9	✓
PH 6	12.6	4.9	7.7	6.9	8.9	0.0	✓
No Pre-heat							
AW 1	11.9	4.7	7.2	7.1	9.4	0.0	✓
AW 2	12.3	5.0	7.3	7.1	9.3	0.5 ± 0.1	✗
AW 3	13.6	5.1	8.4	8.1	10.4	1.4 ± 0.4	✓
AW 4	13.5	5.1	8.5	8.2	10.6	1.9 ± 0.5	✓
AW 5	14.1	4.7	9.3	10.3	12.6	4.3 ± 0.6	✓
AW 6	13.4	5.3	8.2	7.3	9.5	1.0 ± 0.2	✓
AW 7	13.5	5.8	7.7	6.6	7.4	0.0	✓
AW 8	13.3	5.5	7.8	6.6	6.7	0.0	✓
AW 9	13.6	5.0	8.6	8.9	11.5	3.8 ± 0.6	✓
AW 10	14.1	4.4	9.7	11.1	13.5	2.2 ± 0.7	✓
AW 11	12.9	5.4	7.5	6.0	8.4	0.4 ± 0.15	✗
AW 12	11.9	5.2	6.6	5.6	8.1	0.0	✓
AW 13	11.9	5.2	6.8	6.0	8.5	0.0	✓
AW 14	12.3	4.7	7.6	8.4	10.9	0.13 ± 0.06	✓
AW 15	12.9	4.6	8.3	8.9	11.4	1.1 ± 0.3	✓
AW 16	13.7	4.6	9.2	10.2	12.6	6.0 ± 1.1	✓
AW 17	14.1	5.0	9.1	10.7	13.1	6.2 ± 1.2	✓
AW 18	13.5	5.7	7.8	6.7	9.2	1.8 ± 0.4	✗
AW 19	13.6	5.9	7.7	7.5	9.9	2.4 ± 0.5	✓
AW 20	12.9	4.9	8.0	7.6	9.7	0.3 ± 0.14	✗
AW 21	13.5	4.7	8.8	8.6	11.2	2.6 ± 0.6	✓
AW 22	12.1	5.0	7.1	7.0	9.5	0.0	✓

(✓) Presence or absence of delta ferrite was correctly predicted.

(✗) Presence or absence of delta ferrite was incorrectly predicted.

Delta ferrite was not observed in weld PH3 although the FF (Schneider and Kaltenhauser) and CNB (Newhouse) values were slightly above the recommended limits. The application of elevated-temperature preheat treatment, which decreases the cooling rate and allows additional time for the delta ferrite-to-austenite transformation to occur, can be beneficial, as observed with weld PH3, which received 250 °C preheat. The results in Table 6 show that these empirical formulae cannot exclusively be relied upon to accurately predict weld microstructures with

the currently recommended limits, especially where small amounts of delta ferrite are probable. To further improve the predictive accuracy of the empirical formulae for P91 welds, the Schneider, Kaltenhauser, and CNB (Newhouse) recommended limits must be considered, together with use of a preheat temperature above room temperature.

3.5 Thermo-Calc phase-transformation temperatures

The equilibrium solid-state phase-transformation temperatures were calculated using Thermo-Calc version 2022a thermodynamic software. Figure 7 shows the relationship between the ($Ae_4 - Ae_3$) temperature range and amount of delta ferrite in the final microstructure of the welds. Arivazhagan and Kamaraj [4] stated that the probability of delta ferrite retention in the weld increases with a lower value of ($Ae_4 - Ae_3$): Fig. 7 presents results that largely support this statement. Results of previous work conducted on SMAW beads [3] are incorporated in Fig. 7 and show good agreement with the present GMAW results on beads deposited without any preheating.

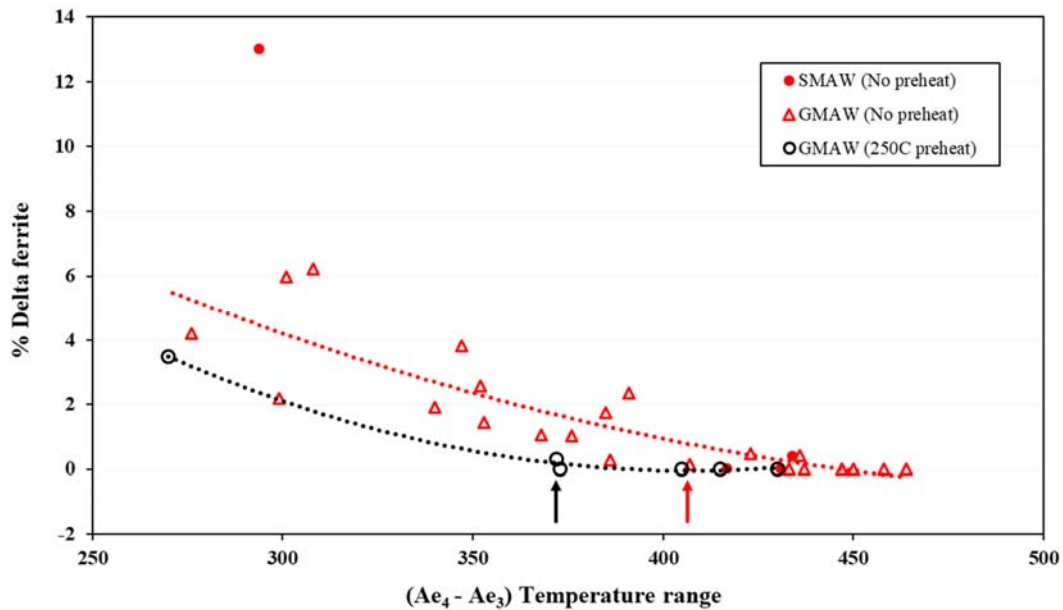


Fig. 7 Relationship between ($Ae_4 - Ae_3$) temperature range and amount of delta ferrite in final microstructure of weld. The red and black arrows indicate the ($Ae_4 - Ae_3$) values necessary to suppress delta ferrite without and with preheating, respectively.

An ($Ae_4 - Ae_3$) temperature range above 415 °C for welds that are not preheated seems to be necessary to suppress delta ferrite in the as-welded microstructure. The required ($Ae_4 - Ae_3$) temperature range decreased to 385 °C when 250 °C preheating was applied. These results indicate that both the chemical composition, which determines the ($Ae_4 - Ae_3$) temperature range, and the cooling rate through this temperature range are important in suppressing delta ferrite in the final as-welded microstructure. The implication is that use of a higher heat input during welding, and the associated lower cooling rate, may result in lower risk of formation of delta ferrite.

4. CONCLUSIONS

In this work, the influence of alloying elements and cooling rate on the presence of delta ferrite in modified 9Cr-1Mo as-welded microstructure was studied. Analysis of weld microstructures and Thermo-Calc-calculated equilibrium transformation temperatures suggested the following conclusions:

- The results clearly demonstrate that compliance of weld metal chemical composition to the AWS A5.28/A5.28M:2020 and EN ISO 21952-A CrMo91 specification ranges does not ensure a fully martensitic as-welded microstructure. For example, Weld AW16 contained 6.0% delta ferrite, yet the composition was within the specification limits.

- Empirical formulae cannot exclusively be relied upon to accurately predict weld microstructures with the currently recommended limits, especially where small amounts of delta ferrite are probable. To further improve the predictive accuracy of the empirical formulae for P91 welds, the Schneider, Kaltenhauser, and CNB (Newhouse) recommended limits must be considered together with a specified elevated-temperature preheat treatment.
- Increases in the estimated ($A_{e4} - A_{e3}$) temperature range above 415 °C without preheating and above 385 °C when 250 °C preheating was applied seemed to reduce the tendency for delta ferrite presence in the as-welded microstructure, as observed in both these GMAW results and previous work on P91 SMAW beads.

5. ACKNOWLEDGEMENTS

We acknowledge the following companies and people for assistance: SecMet for providing the P91 base material; Corney van Rooyen and Maritha Theron at the South African Council for Scientific and Industrial Research (CSIR) for assistance with the laser metal deposition and providing some of the alloying elements; Steinmüller Africa for donating the welding consumable; Prof. Kathy Sole for English editing of this manuscript.

6. DECLARATIONS

Funding: Southern African Institute of Welding

7. CONFLICT OF INTEREST

The authors declare that they have no conflict of interest.

8. REFERENCES

- [1] C. Pandey, M. M. Mahapatra, P. Kumar, and N. Saini, "Some studies on P91 steel and their weldments," *Journal of Alloys and Compounds*, vol. 743, pp. 332-364, 2018.
- [2] X. Zhou, C. Liu, L. Yu, Y. Liu, and H. Li, "Phase Transformation Behavior and Microstructural Control of High-Cr Martensitic/Ferritic Heat-resistant Steels for Power and Nuclear Plants: A Review," *Journal of Materials Science & Technology*, vol. 31, no. 3, pp. 235-242, 2015.
- [3] S. S. Mahlalela and P. G. H. Pistorius, "Investigation of δ -ferrite content in weld metal of modified 9Cr-1Mo electrodes using thermodynamic modelling and quenching experiments," *Welding in the World*, vol. 66, no. 6, pp. 1191-1198, 2022/06/01 2022.
- [4] B. Arivazhagan and M. Kamaraj, "A study on influence of D-ferrite phase on toughness of P91 steel welds," *White Paper, Steel-Grips. Com*, pp. 19-24, 2013.
- [5] B. Arivazhagan and M. Kamaraj, "Metal-cored arc welding process for joining of modified 9Cr-1Mo (P91) steel," *Journal of Manufacturing Processes*, vol. 15, no. 4, pp. 542-548, 2013.
- [6] X. Y. Liu and T. Fujita, "Effect of chromium content on creep rupture properties of a high chromium ferritic heat resisting steel," *ISIJ International*, vol. 29, no. 8, pp. 680-686, 1989.
- [7] B. Arivazhagan, G. Srinivasan, S. K. Albert, and A. K. Bhaduri, "A study on influence of heat input variation on microstructure of reduced activation ferritic martensitic steel weld metal produced by GTAW process," *Fusion Engineering and Design*, vol. 86, no. 2, pp. 192-197, 2011.
- [8] B. Arivazhagan and M. Vasudevan, "A comparative study on the effect of GTAW processes on the microstructure and mechanical properties of P91 steel weld joints," *Journal of Manufacturing Processes*, vol. 16, no. 2, pp. 305-311, 2014.
- [9] Z. Zhang, A. Marshall, and J. Farrar, "Recent developments in welding consumables for P (T) 91 creep-resisting steels," in *Conference Proceedings, International Conference on Integrity of High-Temperature Welds*, 1998, pp. 77-91.
- [10] R. Klueh, "Elevated temperature ferritic and martensitic steels and their application to future nuclear reactors," *International Materials Reviews*, vol. 50, no. 5, pp. 287-310, 2005.
- [11] L. Wang, "Development of predictive formulae for the A1 temperature in creep strength enhanced ferritic steels," The Ohio State University, 2010.

- [12] C. Pandey, M. M. Mahapatra, P. Kumar, and N. Saini, "Homogenization of P91 weldments using varying normalizing and tempering treatment," *Materials Science & Engineering A*, vol. 710, pp. 86-101, 2018.
- [13] R. Faulkner, J. Williams, E. G. Sanchez, and A. Marshall, "Influence of Co, Cu and W on microstructure of 9% Cr steel weld metals," *Materials science and technology*, vol. 19, no. 3, pp. 347-354, 2003.
- [14] M. Sireesha, S. Albert, and S. Sundaresan, "Importance of filler material chemistry for optimising weld metal mechanical properties in modified 9Cr-1Mo steel," *Science and technology of welding and joining*, vol. 6, no. 4, pp. 247-254, 2001.
- [15] A. Barnes, "The effect of composition and heat treatment on the microstructure and mechanical properties of modified 9Cr 1Mo weld metal," TWI Members Report1995.
- [16] J. Onoro, "Martensite microstructure of 9-12% Cr steels weld metals," *Journal of Materials Processing Technology*, vol. 180, no. 1-3, pp. 137-142, 2006.
- [17] R. W. Swindeman, M. L. Santella, P. J. Maziasz, B. W. Roberts, and K. Coleman, "Issues in replacing Cr-Mo steels and stainless steels with 9Cr-1Mo-V steel," *International Journal of Pressure Vessels and Piping*, vol. 81, no. 6, pp. 507-512, 2004.
- [18] D. Olson, "Prediction of austenitic weld metal microstructure and properties," *Welding journal*, vol. 64, no. 10, pp. 281s-295s, 1985.
- [19] M. Sireesha, S. Sundaresan, and S. K. Albert, "Microstructure and mechanical properties of weld fusion zones in modified 9Cr-1Mo steel," *Journal of materials engineering and performance*, vol. 10, no. 3, pp. 320-330, 2001.
- [20] C. Pandey, A. Giri, and M. M. Mahapatra, "Evolution of phases in P91 steel in various heat treatment conditions and their effect on microstructure stability and mechanical properties," *Materials Science & Engineering A*, vol. 664, pp. 58-74, 2016.
- [21] S. Sam *et al.*, "Delta ferrite in the weld metal of reduced activation ferritic martensitic steel," *Journal of Nuclear Materials*, vol. 455, no. 1-3, pp. 343-348, 2014.
- [22] X. Zhou *et al.*, "Effects of cooling rates on δ -ferrite/ γ -austenite formation and martensitic transformation in modified ferritic heat resistant steel," *Fusion Engineering and Design*, vol. 125, pp. 354-360, 2017.
- [23] B. Shanmugarajan, G. Padmanabham, H. Kumar, S. K. Albert, and A. K. Bhaduri, "Autogenous laser welding investigations on modified 9Cr-1Mo (P91) steel," *Science and Technology of Welding and Joining*, vol. 16, no. 6, pp. 528-534, 2011.
- [24] M. Abd El-Rahman Abd El-Salam, I. El-Mahallawi, and M. El-Koussy, "Influence of heat input and post-weld heat treatment on boiler steel P91 (9Cr-1Mo-V-Nb) weld joints Part 1-Microstructure," *International Heat Treatment and Surface Engineering*, vol. 7, no. 1, pp. 23-31, 2013.
- [25] M. R. Spiegel, J. J. Schiller, and R. A. Srinivasan, *Schaum's outline of probability and statistics*. McGraw-Hill Education, 2013.